RL-TR-93-198
In-House Report
September 1993

A CURRENT EVALUATION OF THE DIGITAL BEAMFORMING TESTBED AT ROME LABORATORY

William R. Humbert and Hans Steyskal

APPROVED FOR PUBLIC RELEASE; DISTRIBUTION UNLIMITED.

Rome Laboratory
Air Force Materiel Command
Griffiss Air Force Base, New York

This report has been reviewed by the Rome Laboratory Public Affairs Office (PA) and is releasable to the National Technical Information Service (NTIS). At NTIS it will be releasable to the general public, including foreign nations.

RL-TR-93-198 has been reviewed and is approved for publication.

APPROVED:

DANIEL J. JACAVANCO
Chief, Antennas & Components Division
Electromagnetics & Reliability Directorate

FOR THE COMMANDER:

JOHN K. SCHINDLER
Director of Electromagnetics & Reliability

If your address has changed or if you wish to be removed from the Rome Laboratory mailing list, or if the addressee is no longer employed by your organization, please notify RL (ERAA) Hanscom AFB MA 01731. This will assist us in maintaining a current mailing list.

Do not return copies of this report unless contractual obligations or notices on a specific document require that it be returned.

REPORT DOCUMENTATION PAGE

Form Approved
OMB No. 0704-0188

1. AGENCY USE ONLY (Leave blank)	2. REPORT DATE	3. REPORT TYPE AND DATES COVERED
	September 1993	In-house (July 1992-July 1993)

4. TITLE AND SUBTITLE
A Current Evaluation of the Digital Beamforming Testbed at Rome Laboratory

5. FUNDING NUMBERS
PE 62702F
PR 4600
TA 24
WU 01

6. AUTHOR(S)
William R. Humbert
Hans Steyskal

7. PERFORMING ORGANIZATION NAME(S) AND ADDRESS(ES)
Rome Laboratory (ERAA)
31 Grenier Street
Hanscom AFB, MA 01731-3010

8. PERFORMING ORGANIZATION REPORT NUMBER
RL-TR-93-198

9. SPONSORING/MONITORING AGENCY NAME(S) AND ADDRESS(ES)

10. SPONSORING/MONITORING AGENCY REPORT NUMBER

11. SUPPLEMENTARY NOTES
Rome Laboratory POC: Hans Steyskal/ERAA x-2052

12a. DISTRIBUTION/AVAILABILITY STATEMENT
Approved for public release;
Distribution unlimited

12b. DISTRIBUTION CODE

13. ABSTRACT *(Maximum 200 words)*

The purpose of this report is to provide a recent evaluation of the digital beamforming (DBF) testbed at Rome Laboratory, Hanscom AFB, MA. Section 1 of the report provides a brief introduction to digital beamforming and some of the associated concepts. Section 2 briefly discusses each component of the digital beamforming system (form and function) in a top-down fashion. Section 3 discusses some system limitations associated with the receiver architecture and outlines the techniques used to investigate these limitations. Section 4 contains the measurement results, which show in-phase and quadrature errors approximately 27 dB below the signal, and dc offsets approximately 37 dB below the signal. Third order harmonics are also $\approx$ 37 dB below the signal. Amplitude variation among the channels is $\pm$2dB. Removal of the dc offset error had little effect on a 40 dB Taylor pattern. However, removal of the in-phase and quadrature errors (the dominant errors) greatly improved the pattern. Also included are simple examples of super-resolution of two sources spaced about 1/2 beamwidth apart, and of open-loop adaptive nulling for a 20 dB Taylor pattern.

14. SUBJECT TERMS
Digital beamforming
Adaptive array
Error effects
Error corrections

15. NUMBER OF PAGES
42

16. PRICE CODE

17. SECURITY CLASSIFICATION OF REPORT	18. SECURITY CLASSIFICATION OF THIS PAGE	19. SECURITY CLASSIFICATION OF ABSTRACT	20. LIMITATION OF ABSTRACT
Unclassified	Unclassified	Unclassified	SAR

Contents

Illustrations

Acknowledgements

We would like to thank Dr. Lars Pettersson, Sweden, for illuminating discussions and 1Lt. Warren Brandow for help with the antenna control software and measurements.

A Recent Evaluation of the Digital Beamforming Testbed at Rome Laboratory

1 INTRODUCTION

It is well documented and understood that beamforming with phased arrays requires:

- Co-phasing the array element signals received from the desired direction.
- Applying amplitude control to achieve the desired sidelobe level.
- Summing the weighted array signals to obtain the antenna's beam response in the desired direction.

This is true for both analog and digital beamforming.

In an analog system, the phase of the signals at the elements is controlled by phase shifters or time delays depending on the bandwidth of the signal and the required scan capabilities of the array; the amplitude taper in the array is achieved through a customized feed network designed to realize a certain sidelobe level; the final summing of the weighted element signals is also done by the feed network. The overall performance of the array depends on the precision to which the various parts of the system can be manufactured.

Received for publication 24 September 1993

In a digital system there exists a dedicated processor that accepts a digital representation of the signal at the element, applies the desired amplitude and phase control by means of a single complex multiply, and finally sums the weighted signals to obtain a digital representation of the antenna response. Conceptually, this offers the opportunity to obtain precise control of the array's transfer function starting at the element level. Furthermore, having access to information at the element level allows for the implementation of nonlinear signal processing algorithms designed to greatly enhance the performance of the array. These can provide the flexibility needed in beam pattern control to achieve:

- Improved adaptive pattern nulling and the ability to place multiple nulls in an ECM environment.
- Closely spaced multiple beams as a means of countering high speed, low radar cross section target threats.
- Super resolution to permit multiple targets within one beamwidth to be resolved and accurately tracked to discriminate between spaced decoys and threats.

2 SYSTEM DESCRIPTION

The digital beamforming testbed consists of a receive array, which outputs digitized signals, and two digital signal processing systems, either of which may be used. Figure 1 is a block diagram depicting the testbed configuration as of 24 September 1993. The "off-line" system is based on the Hewlett-Packard computer system and its interface. The "real-time" system consists of the digital beamformer, its interface, a magnitude processing unit (MPU) with a digital-to-analog (D/A) converter , and the Micro Vax III. To explain the basic operation of the testbed, more fully, each of these systems is described.

2.1 Array

The front end of the Digital Beam Forming (DBF) system is a linear array manufactured by General Electric [2]. The array, designed for C-band (5.2-5.7 GHz) receive only operation, consists of 256 straight-arm microstrip dipole elements arranged in 32 columns of 8 elements. Each column constitutes one element of the linear array. To reduce edge effects, the array is surrounded by two lines of dummy elements. The vertical dipoles are printed on both sides of a copper-clad duroid substrate and the elements in each column

are combined in a Wilkinson power combiner giving a relatively narrow elevation pattern. There are a total of 32 receivers: one per element, placed within the array casing.

The element receivers, depicted in Figure 2, use a triple conversion mixing scheme for the RF portion and two A/D converters to generate the digital representation of the signal.

The first stage of mixing is an agile local oscillator (LO) providing an operational bandwidth of 0.5 GHz. After passing through a second LO and a bandpass filter, the final IF is split using a 3 dB power divider. Each signal is then mixed down to baseband; one with the final LO phase shifted by 90°; thus creating the in-phase and quadrature phase components (I and Q). The I and Q components are then amplified, filtered, and finally passed through separate A/D converters. The 10 bit A/D conversion process occurs at a rate of 0.5 MHz which determines the receiver dynamic range and instantaneous bandwidth. This particular receiver architecture provides greater flexibility in choosing the active components necessary to optimize the performance of the receiver. Some of the disadvantages to this choice of receiver architecture are the increase in cost and power consumption.

Once the element voltage responses are digitized they are sent serially via ECL twisted pair cables from the array to the off-line and real-time interfaces. The off-line interface is commonly referred to as the *RACS Box* and the real-time interface will be referred to as the *DBF Interface.*

2.2 RACS Box and DBF Interface

The purpose of any interface is to establish and control the links between two or more devices, and in the process, perform any data transformations necessary to insure the receiving device can comprehend the information being passed. The RACS Box accepts the serial data in offset binary format, and converts it to a digital word containing identifier and control information as well as the datum itself. At this point, it is transferred via the standard IEEE-488 bus to the Hewlett-Packard system for storage. Permanent storage of the antenna data provides a greater flexibility for using various methods of analysis without destroying the original data. The DBF interface is a free running interface. Here, the data are converted from serial to parallel and from offset binary to two's complement,

and then transferred directly to the beamformer through 32 separate ribbon-like cables containing data information only (9 bits I - 9 bits Q). This allows for real-time digital beamforming operation.

2.3 Hewlett Packard Computer System

We do not give details of the computer system peripherals, but rather, briefly list the valuable functions and capabilities of the computer system as a whole. The most important tasks performed include:

- Accepting data from internal or external calibration signals and determining gain and phase errors, DC offset errors, and I/Q imbalance errors.
- Displaying stored element data in various formats (that is, tabular or graphic versions of the element voltage response vs time or frequency).
- Displaying calculated antenna patterns using stored element data.
- Performing any other customized data analysis technique and display results.
- Controlling amplitude, frequency, and modulation of a number of external sources addressable by the HPIB extender (*currently 2 - hardware exists for 1 additional*).
- Controlling antenna mount positioner for automated antenna measurements.

2.4 Digital Beamformer

The digital beamformer, manufactured by Texas Instruments [3], is the specialized computer processor responsible for weighting the array signals properly and summing them to form the desired beam. It employs integer arithmetic, and the quadratic residue number system (QRNS), thus avoiding computational round off errors. The digital beamformer contains four independent inner-product processors operating in parallel, thus allowing for the formation of four independent simultaneous beams.
Relevant data are:

- Input: 64 complex channels (9 bits I, 9 bits Q)
- Output: 4 beams

- Clock Rate: Up to 16 MHz
- Data Rates: in $\simeq$ 20 Gb/sec, out $\simeq$ 2 Gb/sec.
- Performance: 16×10^9 operations/sec.

Since the bandwidth is excessive for many applications, 4, 8, 16 or 32 beams can be multiplexed with a proportionally reduced bandwidth. (The apparent mismatch between the clock rate and number of bits per word of the beamformer and the 32-element array is a consequence of the two systems being built under two independent contracts).

A built-in memory in the beamformer allows capturing of 8192 contiguous time samples on input (*received element signals*) or alternatively, 1024 samples on output (*received beam signals*). These can be sent to the beam controller for data recording and interpretation. The output can also be sent to the magnitude processing unit to examine a real-time analog version of the received signal.

2.5 Magnitude Processing Unit (MPU)

At times it may be desirable or beneficial to have the analog output of the antenna response. The MPU accepts data from one of the beamformers where it is converted to a magnitude (that is, $\sqrt{I^2 + Q^2}$) via a *Pythagorean processor.* This magnitude is then sent to a D/A converter. If the incoming signal is AM modulated, the output of the D/A converter can be displayed graphically on an oscilloscope or aurally in an audio receiver. Both are currently available at the test facility. It should be noted that the magnitude processor can accept data from only one of the four beamforming processors predetermined by the beam controller VAX.

2.6 Beam Controller / MicroVAX III

Again, we do not discuss the peripherals of the VAX but concentrate on the primary functions of the VAX as a controller. They are:

- Controlling the digital beamformer's functions by means of a specially designed command set. Commands include:
  - SETUP - used to run an internal self-test to isolate hardware malfunctions.

  - MODES - used to control beamformer fundamental operations (that is, turn sampling on/off, turn testing on/off, turn processors on/off)
  - DLSAM - used to send a specified sample set from the VAX to the beamformer for scenario testing.
  - DLTAP - used to store a given vector representation of desired element weightings in the beamformer.
  - ULSAM - used to upload a specified number of time samples from the beamformer to the VAX from a specified element.
  - ULDAT - used to upload a specified number of time samples from one of the four beamforming processors to the VAX.
- Performing any calculations necessary for algorithms designed to enhance array performance.
- Executing any specialized data interpretation schemes and display results.

The beamformer is addressable from the VAX through the standard DRV-11 interface. All commands are sent to the beamformer and all data are received from the beamformer using MATLAB, a software package available from "The Math Works".

3 SYSTEM LIMITATIONS

Obviously, a good knowledge of system limitations that may inhibit the performance of the array is highly desirable. Determining system errors by examining far field pattern data may be difficult or impractical, and, typically, built-in test equipment is used to isolate system errors. However, in a DBF system where information on the element level is preserved, isolation of some of the internal errors is made much easier. Furthermore, assigning a portion of the beam controller's time for monitoring element errors is easily implemented. The specific array limitations to be discussed include:

- Insertion Gain/Phase Differences
- I/Q Imbalance Errors
- DC Offset Errors
- Higher Order Harmonics

– Receiver Noise Differences

These limitations have several effects on an incident signal. Consider a signal $x_n^{in}(t)$ incident on the n^{th} element of the array expressed as

$$x_n^{in}(t) = \Re\left\{e^{j(\omega+\Omega)t}\right\} \tag{1}$$

where ω is the angular frequency of the carrier, Ω is the angular frequency of the signal, and $\Re\{\}$ denotes the real part of the expression. After three stages of mixing followed by the I and Q signal generation circuit the normalized complex output is

$$x_n^{out}(t) = (1+\epsilon_n^A)e^{j\Omega t} + \epsilon_n^{DC} + \epsilon_n^{IQ}e^{-j\Omega t} + \sum_{|m|>1}^{\infty} \epsilon_n^H e^{jm\Omega t} \tag{2}$$

where subscript n represents the n^{th} element; ϵ_n^A is a complex constant representing the amplitude error (insertion gain, phase) caused by differences between the receiver modules; ϵ_n^{DC} is a complex constant representing the dc offset caused by the video amplifier, low pass filter, and A/D converter; ϵ_n^{IQ} is a complex constant representing the I/Q imbalance caused by differences in the amplitude and/or quadrature phase (90°) between the I and Q channels; and ϵ_n^H is a complex constant representing the higher order harmonics caused by device nonlinearities. It should be noted that the last term in Eq. (2) includes all possible higher order harmonics. It assumes nothing about the nature of the nonlinearities, for example, whether they are quadratic or cubic [4]. However, for this particular system, we are interested in only the third order harmonic as it is most predominant in the output signal. Thus, the final output signal is written

$$x_n^{out}(t) = (1+\epsilon_n^A)e^{j\Omega t} + \epsilon_n^{DC} + \epsilon_n^{IQ}e^{-j\Omega t} + \epsilon_n^H e^{j3\Omega t} \tag{3}$$

The limitations of the digital beamforming testbed are quantified andtheir effect on the array's performance determined using frequency domain spectral analysis and eigen-analysis techniques.

3.1 Spectral Analysis

Identifying and isolating the components of Eq. (3) using time domain techniques would be difficult and require special test equipment. However, a frequency domain analysis leads to a straightforward method of isolating and quantifying the various signal components. A brief discussion is included here to supplement the measured results.

Clearly, the terms in Eq. (3) have distinct frequency components; thus, using the Fourier transform relation

$$\mathcal{F}\left\{x_n^{out}(t)\right\} = X_n^{out}(\omega) \tag{4}$$

where $\mathcal{F}\{\}$ is the Fourier transform operator, makes it possible to isolate each of the components in Eq. (3). For example, consider again the incident signal with carrier frequency ω and modulation frequency Ω. Using Eq. (3) in Eq. (4) we can write the following relationships for the n^{th} channel

$$1 + \epsilon_n^A = X_n^{out}(\omega)\,|_{\omega=\Omega} \tag{5}$$

$$\epsilon_n^{DC} = X_n^{out}(\omega)\,|_{\omega=0} \tag{6}$$

$$\epsilon_n^{IQ} = X_n^{out}(\omega)\,|_{\omega=-\Omega} \tag{7}$$

$$\epsilon_n^{H} = X_n^{out}(\omega)\,|_{\omega=3\Omega} \tag{8}$$

These relations allow for a convienient method of isolation, identification, and quantification of the described errors. However, because the signal is sampled at a fixed rate (500 kHz), a suitable value for Ω must be chosen carefully when making measurements. Clearly, with no modulation, that is, $f_\Omega = 0$ Hz, complete ambiguity exists and no isolation occurs. Other choices of f_Ω to avoid are $\frac{1}{2}$ and $\frac{1}{4}$ of the A/D sampling frequency. These give rise to partial ambiguities in error isolation. Figures 3-5 are graphical depictions of error isolation with various choices of f_Ω. Obviously, f_Ω must be chosen small enough so that the highest frequency component of interest falls within the bandwidth of the spectrum and is not undersampled according to the Nyquist criterion. For all of the measured results to be discussed later, we chose $f_\Omega = 15.625$ kHz, that is, $\frac{1}{32}$ of the A/D sampling frequency, and used 512 time samples, which corresponds to 13 periods. It should be noted that only an integral number of periods of the signal should be sampled for the FFT to produce a clean line spectrum. An example of the spectral line spreading that would otherwise occur is shown in Figure 6 for $f_\Omega = \frac{1}{7}$ A/D sampling frequency.

3.2 Eigen-analysis

An alternative method of analyzing the array signals is to use the covariance matrix. An eigen-analysis of this matrix provides valuable insights that complement a frequency domain analysis. The main features are summarized here for reference when discussing the measured results. For a simple but instructive example, consider two signals incident

on an antenna array as shown in Figure 7. The vector $a = (a_1, a_2, \ldots, a_M)^t$ represents the complex element amplitudes due to signal A at frequency ω_a. Similarly, the vector $b = (b_1, b_2, \ldots, b_M)^t$ is the complex element amplitudes due to signal B at frequency ω_b. The vector $n(t) = [n_1(t), n_2(t), \ldots, n_M(t)]^t$ represents the thermal noise components in each of the receiver channels, the vector $w = (w_1, w_2, \ldots, w_M)^t$ is the imposed element weighting for the desired pattern, and ^{t} denotes transpose. The beam output power thus can be written

$$P = \overline{|w^t [ae^{j\omega_a t} + be^{j\omega_b t} + n(t)]|^2} \tag{9}$$

where the overbar denotes time average.

Assuming

1) the signals A and B are uncorrelated

2) equal noise in all channels, that is, $\overline{n_i^2(t)} = n_0$ leads to

$$P = w^t R w^* \tag{10}$$

where the covariance matrix

$$R = n_0 I + aa^\dagger + bb^\dagger \tag{11}$$

and where I denotes the identity matrix, * the complex conjugate, and † the complex conjugate transpose.

Many array signal processing techniques use the covariance matrix R and are best understood in terms of its eigen-analysis.

The matrix R is Hermitian; and thus its eigenvalues λ_i are real and its eigenvectors e_i orthogonal. We shall assume the λ_i's are ordered in decreasing magnitude and the e_i's are normalized. This leads to simple expressions for R and R^{-1}

$$R = \sum_{i=1}^{M} \lambda_i e_i e_i^\dagger \tag{12}$$

$$R^{-1} = \sum_{i=1}^{M} \frac{1}{\lambda_i} e_i e_i^\dagger \tag{13}$$

Our covariance matrix has a very particular structure and therefore an eigenvector expansion of R as given by Eq. (11) leads to

$$R = \underbrace{\sum_{i=1}^{2} \lambda_i e_i e_i^\dagger}_{\textit{signal subspace}} + \underbrace{n_0 \sum_{i=3}^{M} e_i e_i^\dagger}_{\textit{noise subspace}} \tag{14}$$

The expansion can be shown to have the following characteristics:

- only the first two eigenvalues differ, (since there are only two external signals)
- remaining $M-2$ eigenvalues are all equal: $\lambda_i = n_0$, $i > 2$,
- the eigenvector expansion splits R into a 2-dimensional ***signal subspace*** and an orthogonal $(M-2)$-dimensional ***noise subspace***,
- the signal subspace spanned by $\{e_1, e_2\}$ contains the signal vectors a, b,
- $\lambda_1 \simeq n_0 + |a|^2$, $\lambda_2 \simeq n_0 + |b|^2$ when $|a^\dagger b| \ll |a||b|$, that is, for strong signals the eigenvalues equal the powers of A and B, when they are separated by more than a beamwidth.
- when $n_0 \to 0$ the matrix R becomes singular. Consequently, for large signal/noise ratios, R will be nearly singular and difficult to invert numerically.
- these characteristics extrapolate directly to a different number of signals (other than two).

The inverse of R is similarly

$$R^{-1} = \sum_{i=1}^{2} \frac{1}{\lambda_i} e_i e_i^\dagger + \frac{1}{n_0} \sum_{i=3}^{M} e_i e_i^\dagger$$

$$= \frac{1}{n_0} I - \sum_{i=1}^{2} \left(\frac{1}{n_0} - \frac{1}{\lambda_i} \right) e_i e_i^\dagger \tag{15}$$

that is, the inverse is simply the identity matrix minus a projection on signal space.

To demonstrate the above analysis let us consider adaptive pattern nulling based on sample matrix inversion. We assume again a desired signal A and a strong interfering signal B. Following Applebaum [1] we sample the array signals in the absence of A to form the covariance matrix

$$R = n_0 I + bb^\dagger \tag{16}$$

and then compute the optimal weights w from

$$w^* = R^{-1} s \tag{17}$$

where the array steering vector s corresponds to the desired signal direction, that is,

$$s = \frac{a}{|a|} = \hat{a} \tag{18}$$

From this analysis we now obtain

$$R = \lambda_1 e_1 e_1^\dagger + n_0 \sum_{i=2}^{M} e_i e_i^\dagger \tag{19}$$

with

$$e_1 = \frac{b}{|b|} = \hat{b}$$

$$\lambda_1 = n_0 + |b|^2 \gg n_0 \tag{20}$$

leading to

$$R^{-1} = \frac{1}{n_0} I - \left(\frac{1}{n_0} - \frac{1}{\lambda_1}\right) \hat{b}\hat{b}^\dagger \simeq \frac{1}{n_0}\left(I - \hat{b}\hat{b}^\dagger\right) \tag{21}$$

Substituting this in Eq. (17) we find, using Eq. (18)

$$w^* = R^{-1} s \simeq \frac{1}{n_0}\left[\hat{a} - \left(\hat{b}^\dagger \hat{a}\right)\hat{b}\right] \tag{22}$$

The first term of the right hand side of Eq. (22) corresponds to the original quiescent pattern and the last term corresponds to a superimposed sinc-beam of proper amplitude so as to cancel the quiescent pattern in the direction of B. This shows that under idealized conditions the adapted pattern essentially equals the quiescent pattern except for a very localized perturbation around the interference direction.

However, under less ideal conditions, the noise eigenvalues may not all be equal. This may happen if the number of samples is too small or if the receiver channels differ. The derivation above shows that in this case it will not be possible to write R^{-1} in the form of Eq. (21) that is, in terms of an identity matrix and a single vector product. Consequently, the quiescent pattern structure will be lost in the weight vector w and thus in the adapted pattern. This can indeed be observed in practical systems.

The well known *MUSIC* algorithm (multiple signal classification,[5]), used for direction finding, is also easily understood in terms of an eigen-analysis of the covariance matrix. Considering the same example as before of two plane wave signals A and B incident from θ_a and θ_b, the covariance matrix can again be written as [Eq. (14)]

$$R = \sum_{i=1}^{2} \lambda_i e_i e_i^\dagger + n_0 \sum_{i=3}^{M} e_i e_i^\dagger \tag{23}$$

The second term in Eq. (23) corresponds to noise subspace and is denoted by R_n, that is,

$$R_n = \sum_{i=3}^{M} e_i e_i^{\dagger} \tag{24}$$

We now form a steering vector $s(\theta)$, corresponding to a plane wave incident from angle θ and project s onto the noise subspace. When scanning θ we note that for the particular angles θ_a and θ_b the projections

$$R_n s(\theta_a) = R_n s(\theta_b) = 0, \tag{25}$$

in view of the orthogonality between the signal and noise subspaces. Thus, the scan function

$$f(\theta) = \frac{1}{s(\theta)^{\dagger} R_n s(\theta)} \tag{26}$$

will show strong maxima at the incident signal directions. This in essence is the *MUSIC* algorithm.

4 MEASURED RESULTS

This section contains the measured results and documents the digital beamforming testbed performance. It includes the quantification of the errors and their effects on a low sidelobe antenna pattern as well as results from the adaptive nulling and super resolution methods discussed earlier. **All figures are attached to the end of this section.**

4.1 Error Levels and Effects

To quantify the error levels, the array was illuminated by a plane wave with fm-modulation equal to 15.625 kHz, as stated earlier. The transmitter power was adjusted so that the channel with the highest gain was close to, but not saturated. A total of 512 consecutive time samples of each element signal, represented by Eq. (3), were then stored so that a complete spectral analysis could be performed using Eqs. (4)–(8). Figure 8 illustrates the amplitude variation and error levels determined by the spectral analysis. There is a ± 2 dB amplitude variation among the channels. More notably, the channels are dominated by the I/Q errors, which on average are approximately -27 dB below the signal. Similarly, the dc offsets are on average -37 dB below the signal. It should be noted however, the dc

offsets comprise two components; one input power independent (from the A/D converters) and one input power dependent (from the video amplifiers). The measurement reflects the combination of the two. With no signal present,the dc offsets due to the A/D converters are on average -44 dB relative to max A/D output. The third order harmonics present in the channels are also shown and on the average are approximately -37 dB below the signal. Figure 9 is a similar plot illustrating the insertion phase of the channels, which apparently is a random distribution although the receivers are identical. Figure 10 is the measured thermal noise in each of the channels. The average noise power is approximately -47 dB relative to max A/D output. More importantly though, there are differences in the noise powers among the channels, and the associated effects will be addressed later.

The effects of these errors on array performance are assessed by eliminating them one by one and observing the corresponding improvements on a 40 dB Taylor pattern. The gain and phase differences, that is, ϵ_n^A in Eq. (3), are corrected by a single complex multiply done by the digital beamformer in the time domain. The multiplier $(1 + \epsilon_n^A)^{-1}$ is directly available from Eq. (5). The remaining errors are more readily handled in the frequency domain, where they are well isolated and can be suppressed by a digital *notch filter*. Thus to remove one particular error, the sequence of time samples was Fourier transformed, the spectral line corresponding to that error was suppressed and the cleaned spectrum was Fourier transformed back to the time domain. This operation was performed for each of the 32 elements. The resultant, partially and fully corrected array patterns are shown in Figures 11-13; each compared with the quiescent pattern.

Figure 11 shows that removal of the dc component has little or no effect on the pattern. This is due to an averaging out of the uncorrelated dc offsets in the 'beam' response. However, Figure 12 shows a great change in the pattern when the I/Q errors are removed. This should be expected as they are the dominant errors in the channels (see Figure 8). Finally, Figure 13 exhibits a near theoretical antenna pattern after additional corrections for the third order harmonics. It would seem that full array performance is restored with the removal of these array limitations.

Figures 14-16 show more recent and complete measurements of gain variations and error levels for the 32 channels over the frequency band of the array. Compared to the data in Figure 8, which were taken 6 months earlier, there is now a higher amplitude variation among the channels and the errors are now dominated by the dc offset and not the I/Q component as before. This is most likely attributed to a change of the LO unit or,

also, to "aging" of the array. Unfortunately, this matter could not be resolved properly due to time constraints.

4.2 Super-Resolution

As stated earlier, the availability of the individual array element signals allows for a host of non-linear signal processing algorithms to be implemented. One such algorithm that makes use of the covariance matrix as described earlier is the commonly known MUSIC algorithm designed to determine the direction of arrival (DOA) of uncorrelated signals. The digital beamforming testbed was used to demonstrate this algorithm. Figure 17 is the measured result for two signals approximately 10° apart plotted according to Eq. (26). The sharp peaks correspond to the incident directions of the two signals. However, the signals, separated by more than a beamwidth ($\simeq 4°$), could have been resolved using a conventional beam with less accuracy. A more interesting case is for signals separated by less than a beamwidth, requiring *super resolution*, which also was investigated. Figure 18 shows the measured result of the experiment with two signals separated 1.7° apart ($\simeq 0.4$ beamwidth), and compares with the responses obtained by a scanned conventional beam or a monopulse beam. Clearly, only the MUSIC algorithm is able to resolve the sources for this case. In these experiments, only the gain and phase errors were corrected, and the powers of the sources were 40 dB above the noise.

4.3 Adaptive Nulling - SMI

Sample matrix inversion (SMI) is another array signal processing algorithm that uses the covariance matrix. It is designed to adaptively null all interference signals contained in the covariance matrix. It offers the fastest convergence rate; requiring only the time needed to sample the interference signals plus the time to invert the covariance matrix. The digital beamforming testbed was again used to demonstrate adaptive nulling. The optimum weights are given by

$$w^* = R^{-1}s \tag{27}$$

as stated earlier. For the experiment the covariance matrix was calculated using

$$R = \frac{1}{M}\sum_{1}^{M} x_m x_m^\dagger \tag{28}$$

where x_m is a 32 element column vector containing the m^{th} time sample from each of the array elements, and again † represents complex conjugate-transpose. It should be noted for this experiment the vector x contains only interference sources (Applebaum's method), and 256 samples were used to estimate the covariance matrix. Figure 19 is the measured adapted pattern and the corresponding eigenvalue distribution for a single narrowband jammer located at $-10°$ off broadside. Note that the pattern is the **measured received jammer power**. The steering vector s is chosen to maximize the received desired signal at broadside with a 20 dB Taylor taper imposed. Thus, we expected a null at broadside and a mainbeam at $-10°$ when the array is scanned and only the jammer is on. Obtaining the adapted response in this way provides a direct measure of jammer cancellation. The main beam corresponds to maximum received jammer power and the null to jammer cancellation. Figure 19 illustrates a jammer cancellation of 59 dB which is the full dynamic range of the system.

The resultant adapted pattern in Figure 19 does not yield 20 dB sidelobes. This is explained by the covariance matrix eigenvalues shown also in Figure 19. Ideally, there should be only one large eigenvalue and the rest should be of equal, low magnitude. In our case, the relatively large second, third, and fourth eigenvalues represent array errors (dc offset, I/Q, third harmonic) and remaining eigenvalues represent different noise figures of the receiver channels. As a result, the weight vector w cannot be written in the idealized form of Eq. (22), and the quiescent pattern structure is lost. A correction of the three dominant array errors leads to the eigenvalue distribution shown in Figure 20. However, the noise eigenvalues still differ and thus would spoil the sidelobe structure of any adapted pattern.

However, by diagonally loading the covariance matrix and thus artificially increasing the noise component, we can make the noise structure more uniform. Figure 21 is the measured adaptive pattern and the corresponding eigenvalue distribution as a result of diagonal loading. Note that the jammer cancellation has decreased by 2 dB. This is to be expected with a decrease in jammer to noise ratio.

This demonstrates the capability of simultaneously adaptively nulling the interference *and* maintaining low sidelobe performance. Again in this experiment, only the gain and phase errors were corrected and the SNR of the jammer was approximately 40 dB.

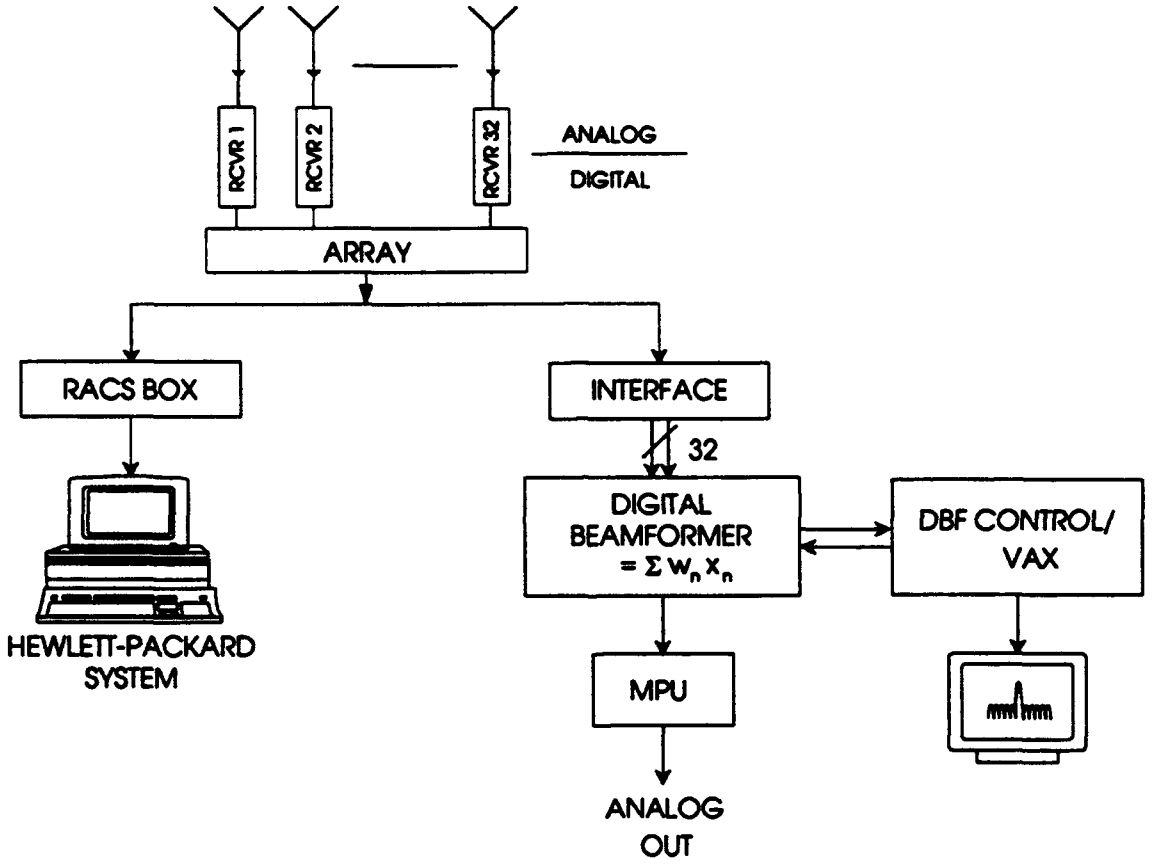

Figure 1: Block diagram of the Digital Beamforming Testbed at Rome Laboratory

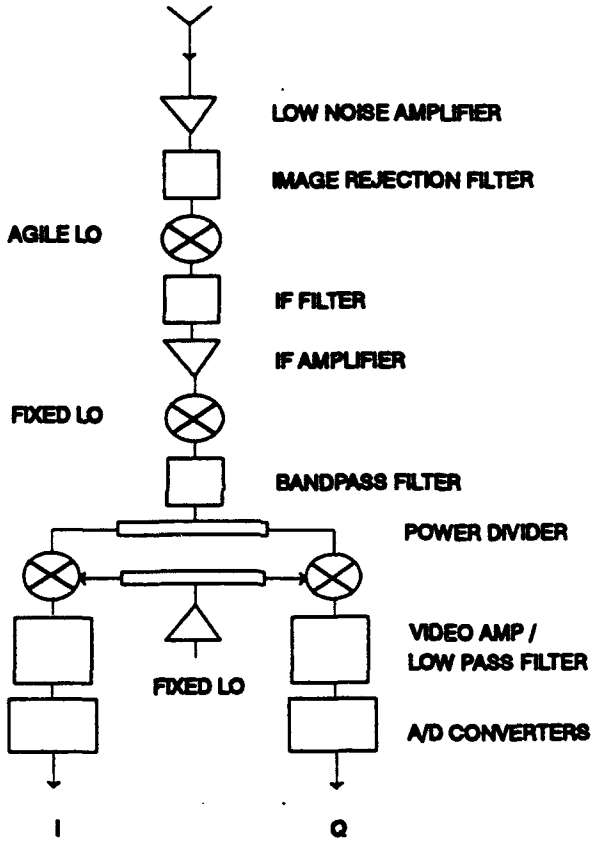

Figure 2: Block diagram of an element receiver

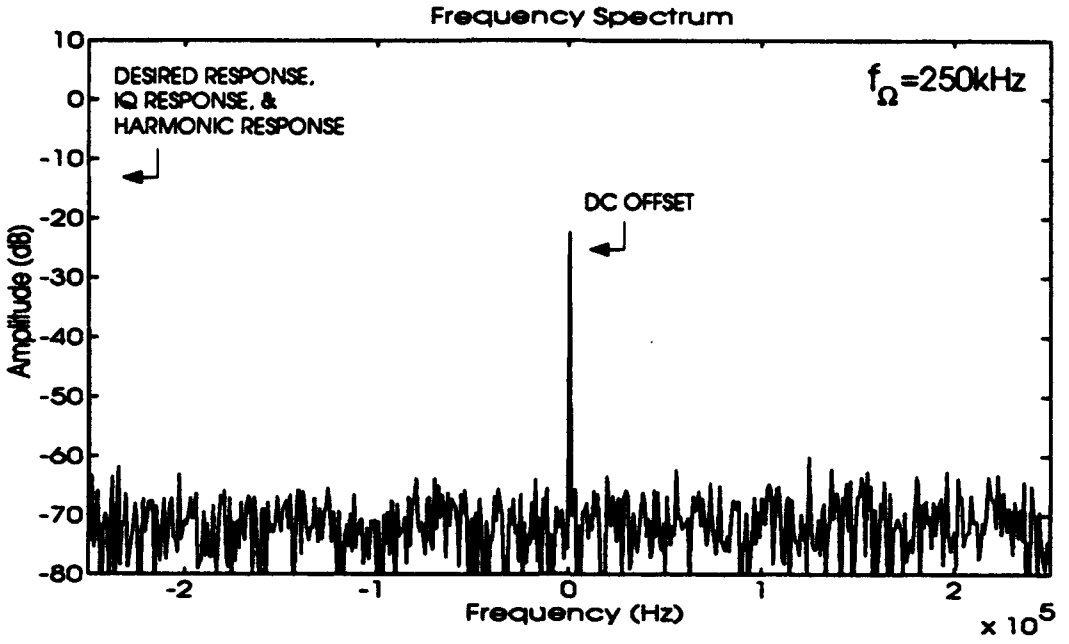

Figure 3: Spectrum for $\frac{1}{2}$ A/D sampling frequency

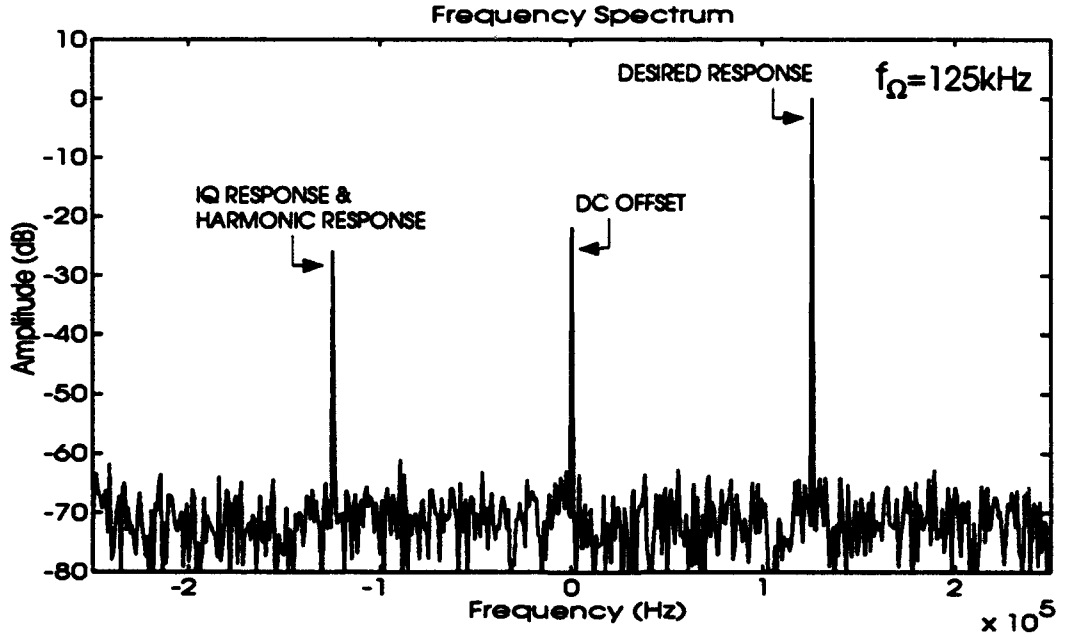

Figure 4: Spectrum for $\frac{1}{4}$ A/D sampling frequency

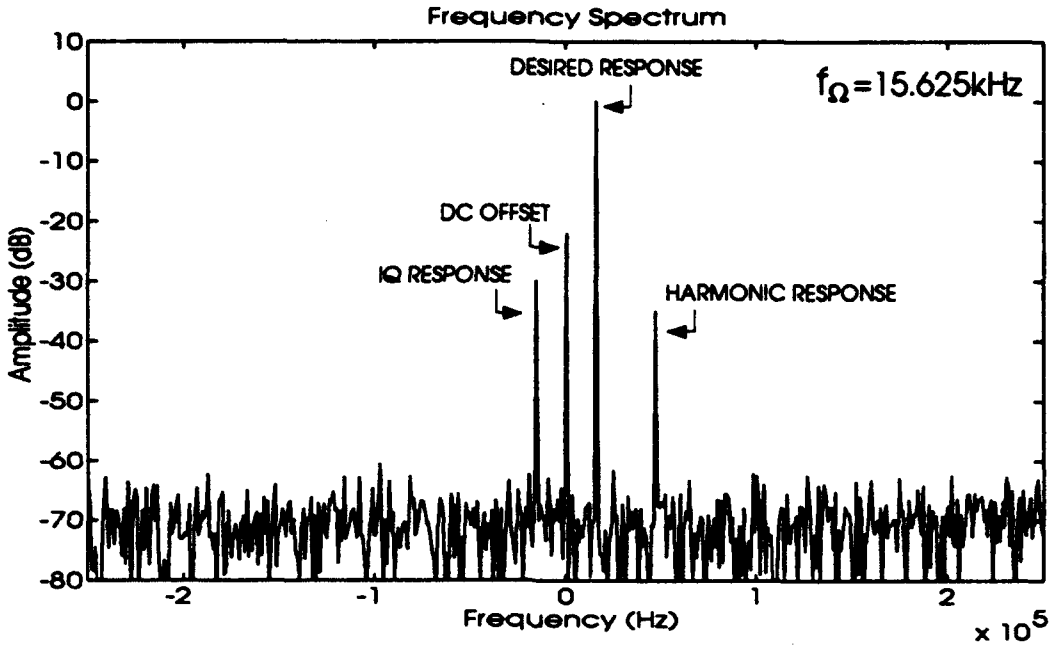

Figure 5: Spectrum for $\frac{1}{32}$ A/D sampling frequency

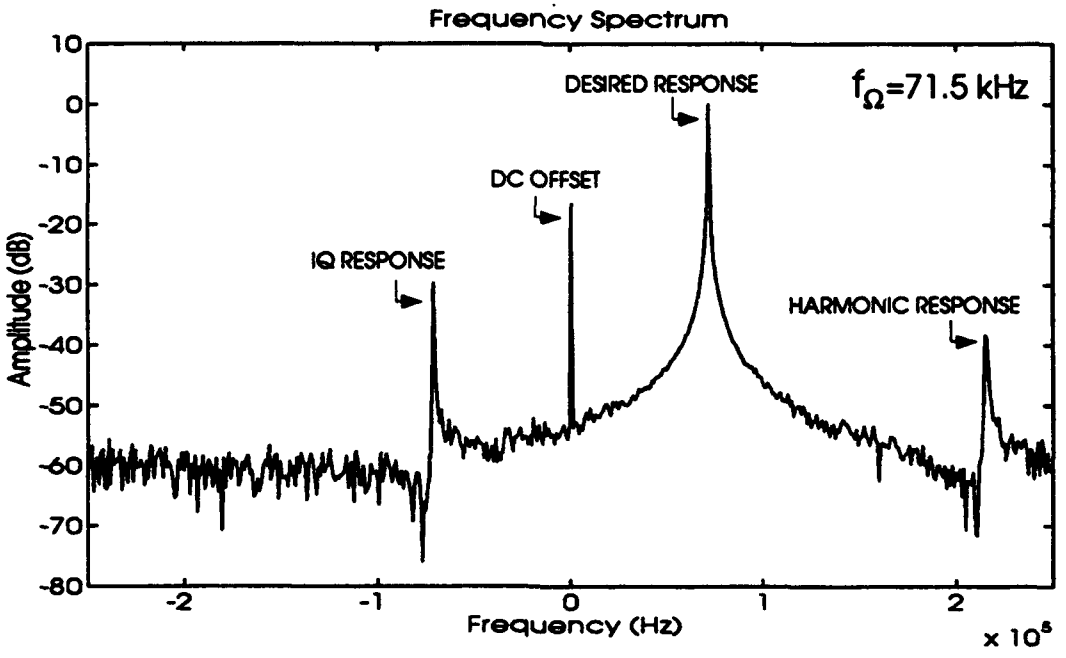

Figure 6: Spectrum for $\frac{1}{7}$ A/D sampling frequency - note spreading of spectral lines

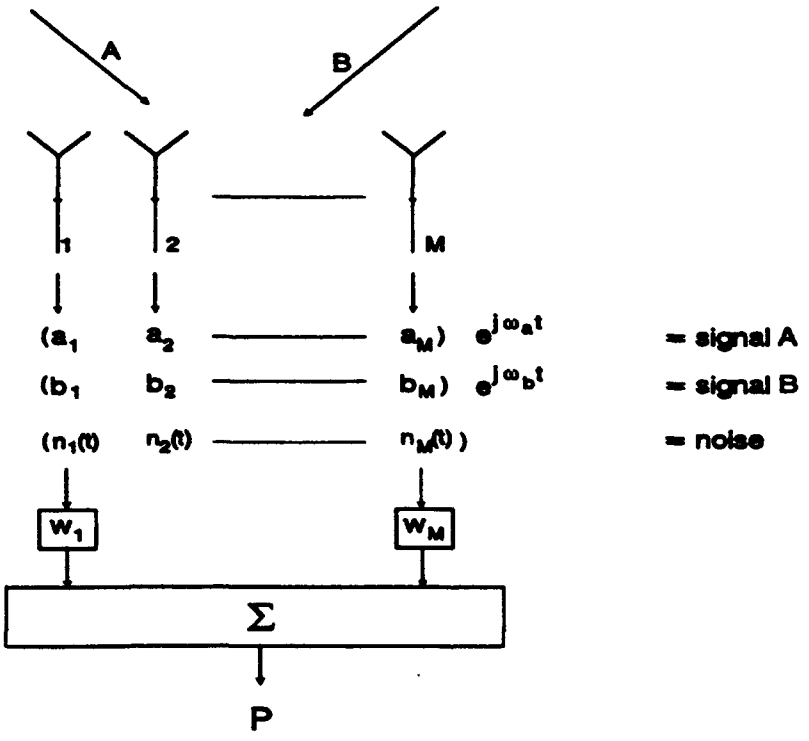

Figure 7: Two signals incident on antenna array

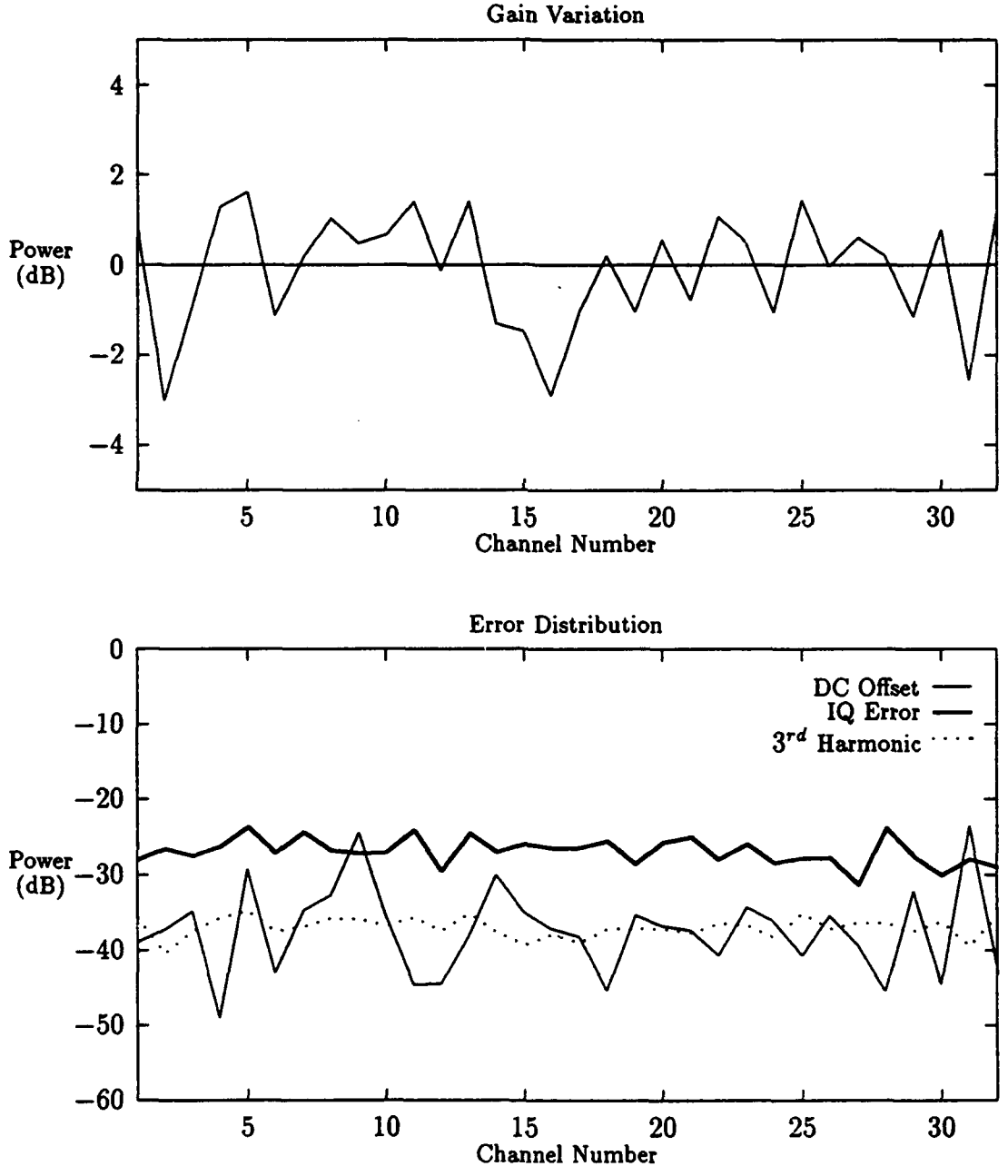

Figure 8: Measured Gain Variations and Error Levels

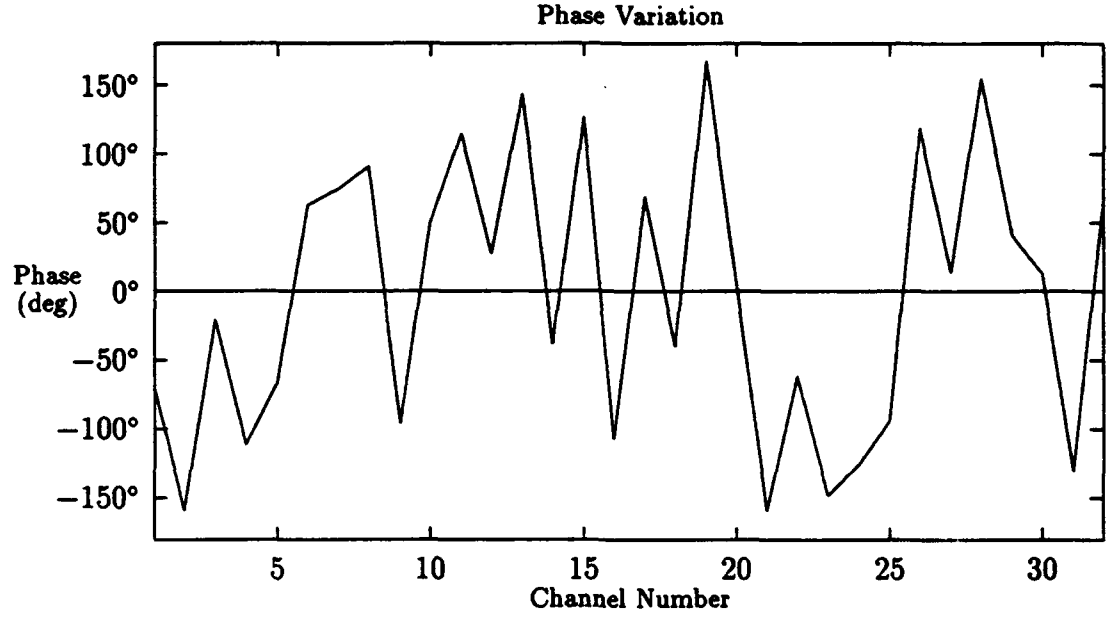

Figure 9: Measured Phase Variation

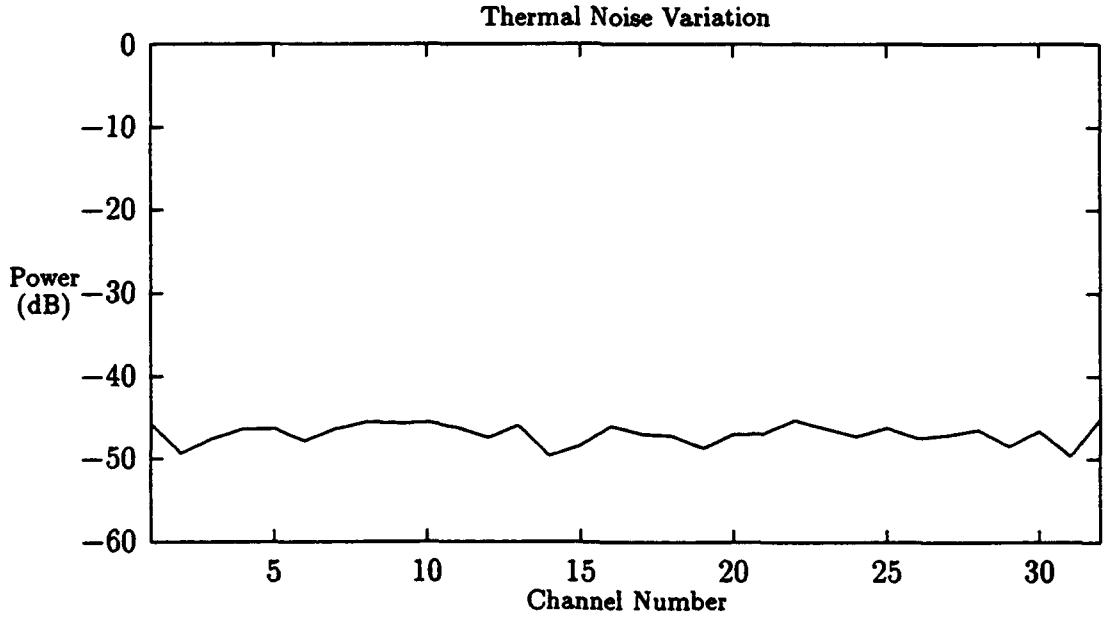

Figure 10: Measured Thermal Noise

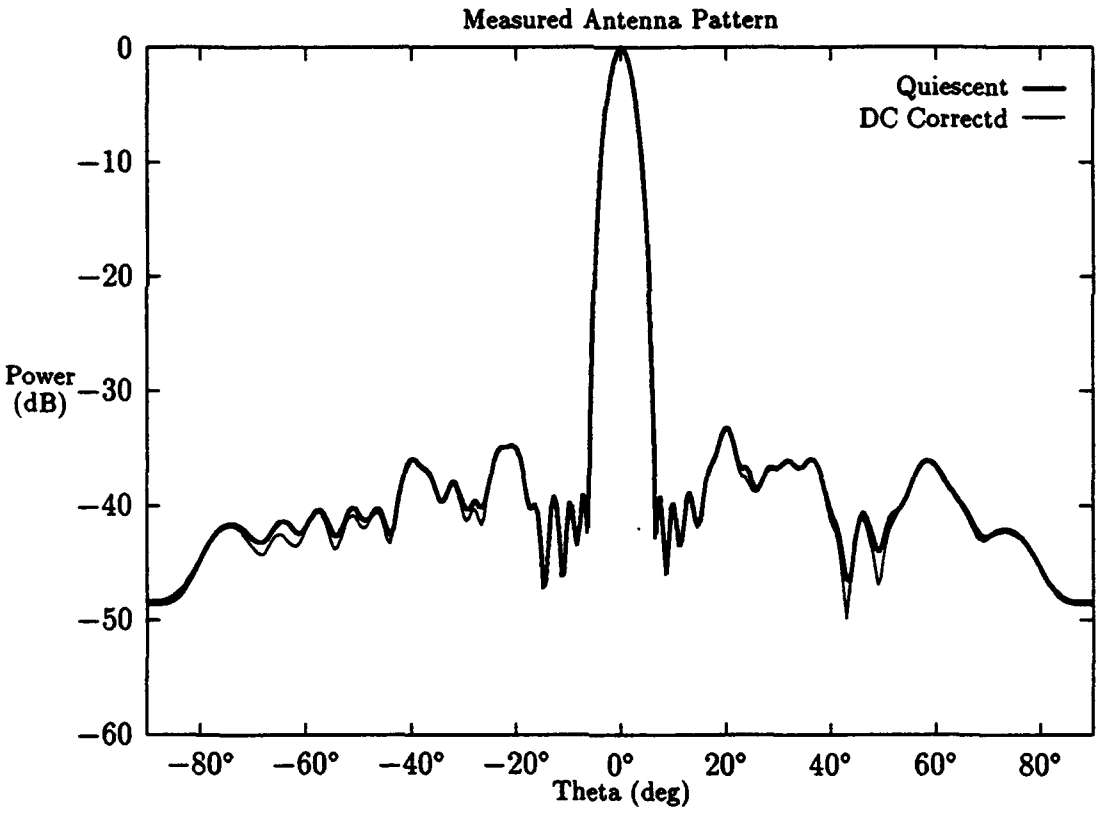

Figure 11: Measured 40 dB Taylor - dc Corrected

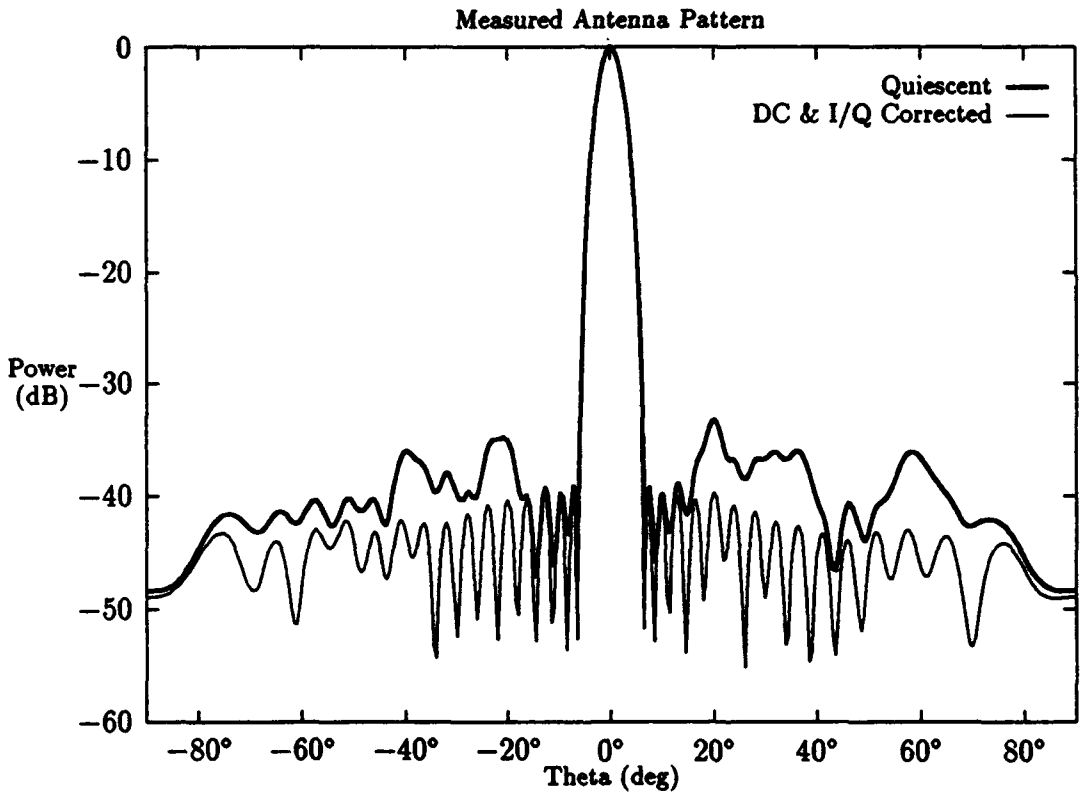

Figure 12: Measured 40 dB Taylor - dc and I/Q Corrected

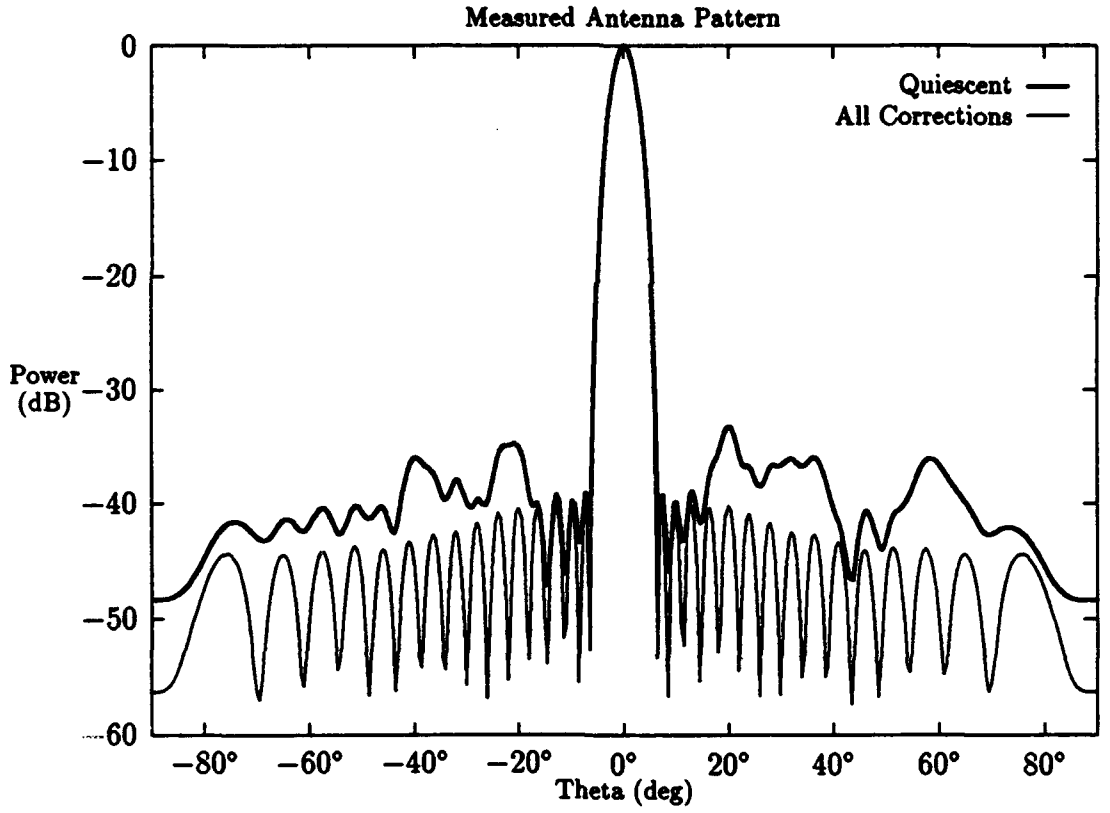

Figure 13: Measured 40 dB Taylor - dc, I/Q and Third Harmonic Corrected

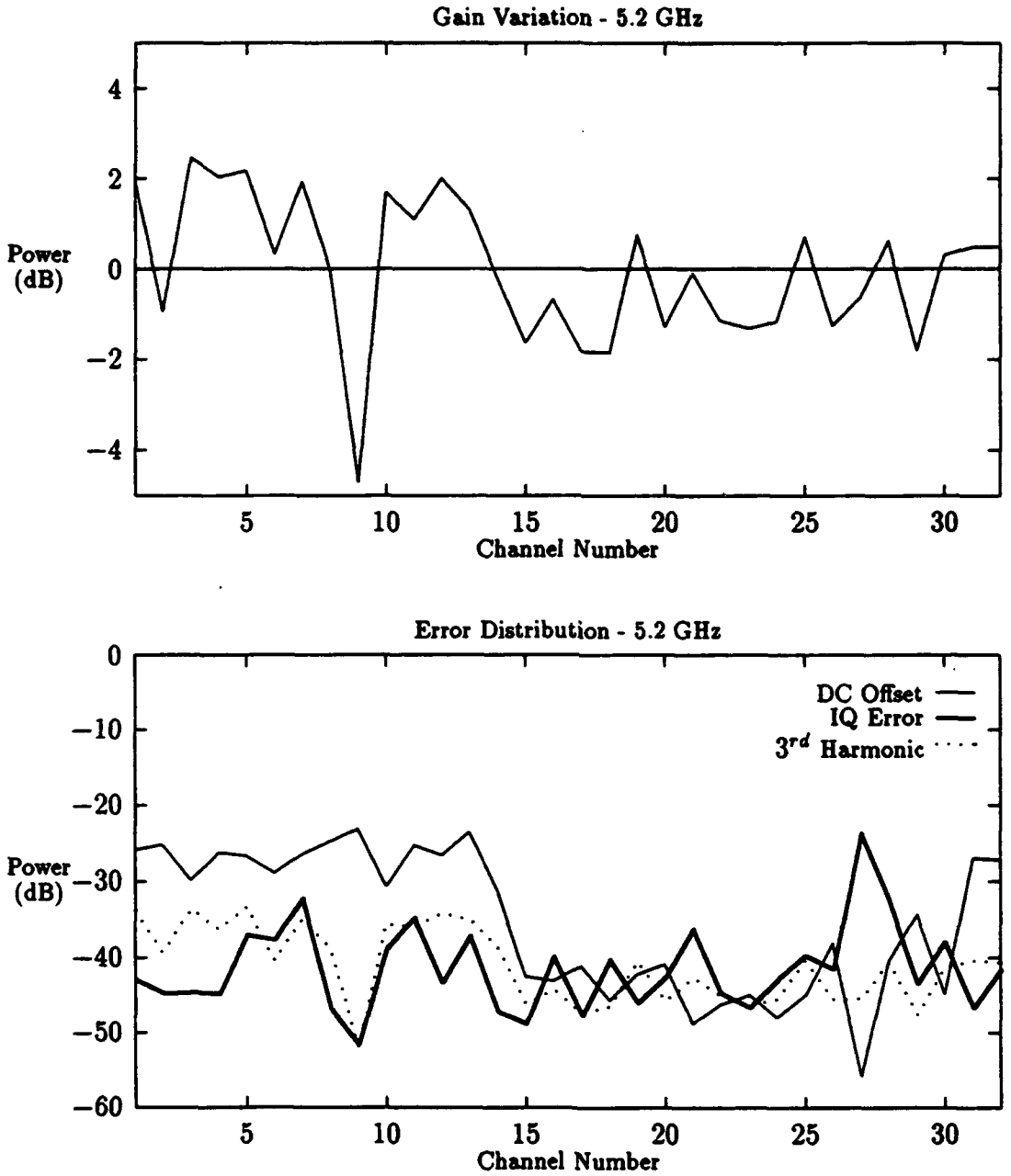

Figure 14: Measured Gain Variations and Error Levels - 5.2 GHz

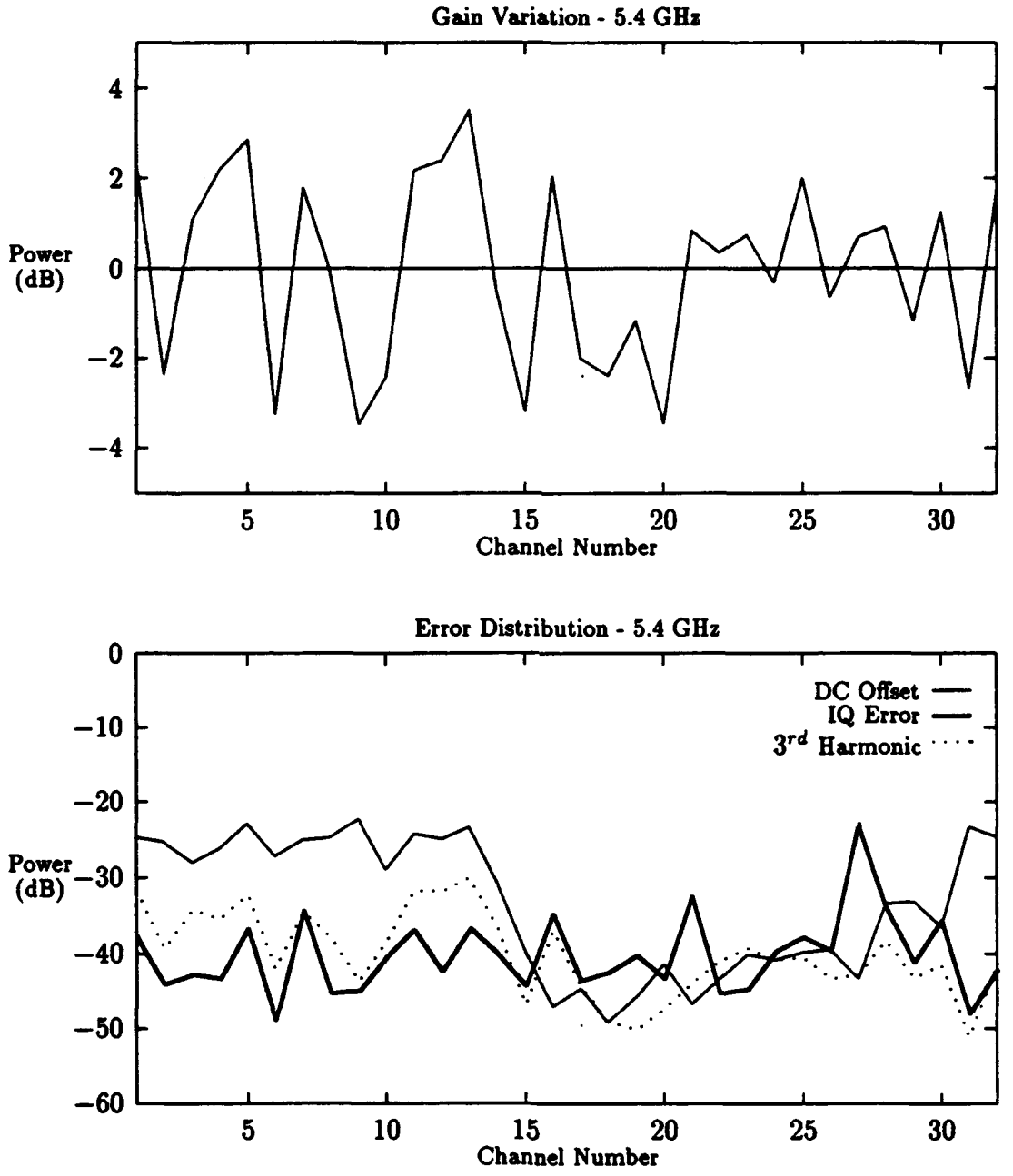

Figure 15: Measured Gain Variations and Error Levels - 5.4 GHz

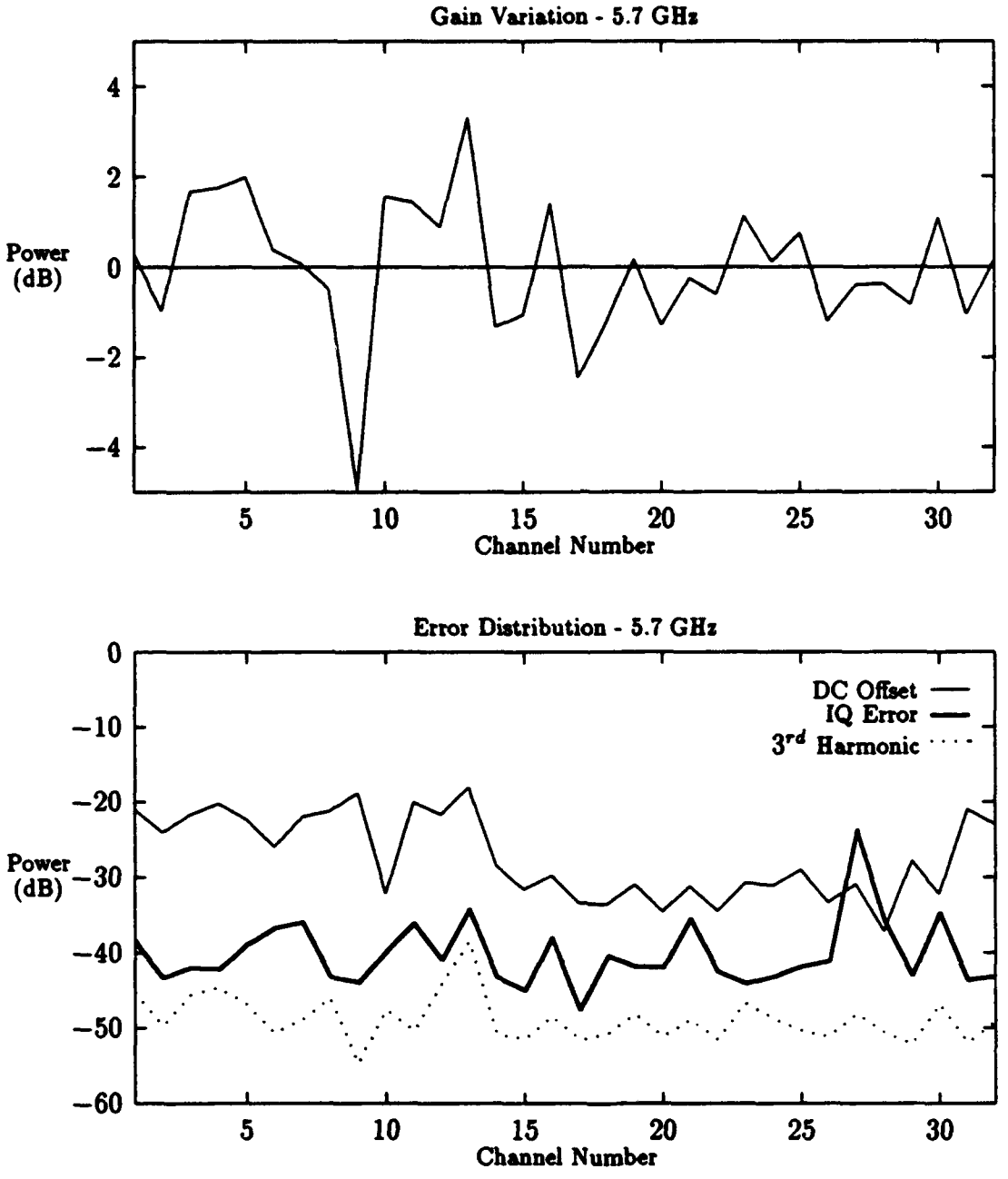

Figure 16: Measured Gain Variations and Error Levels - 5.7 GHz

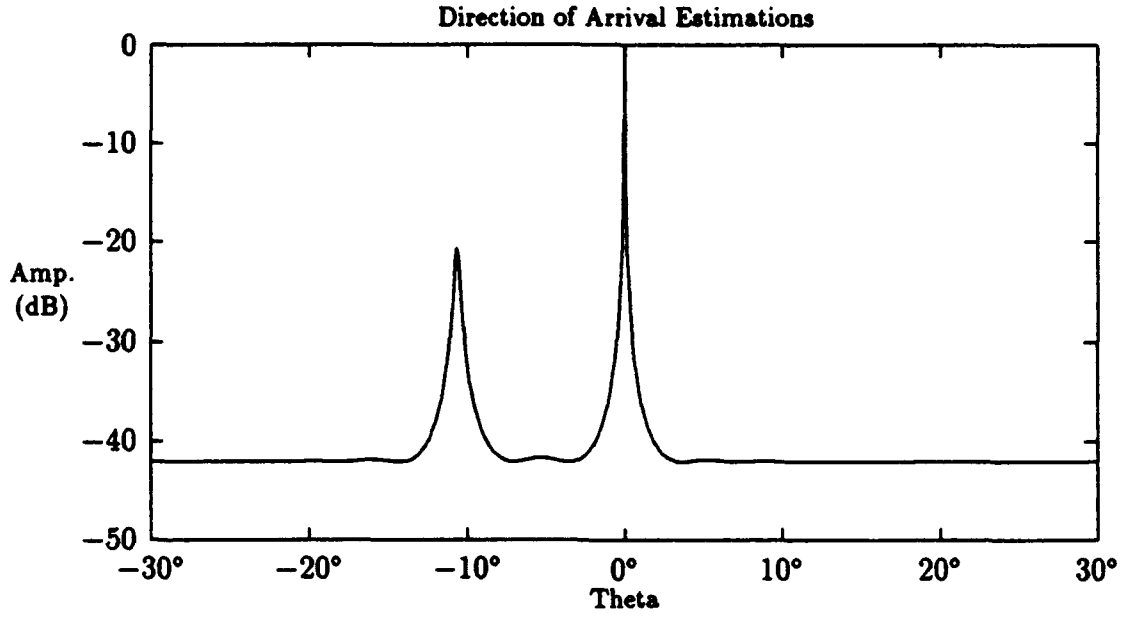

Figure 17: Measured MUSIC Algorithm Response - Sources 10° apart

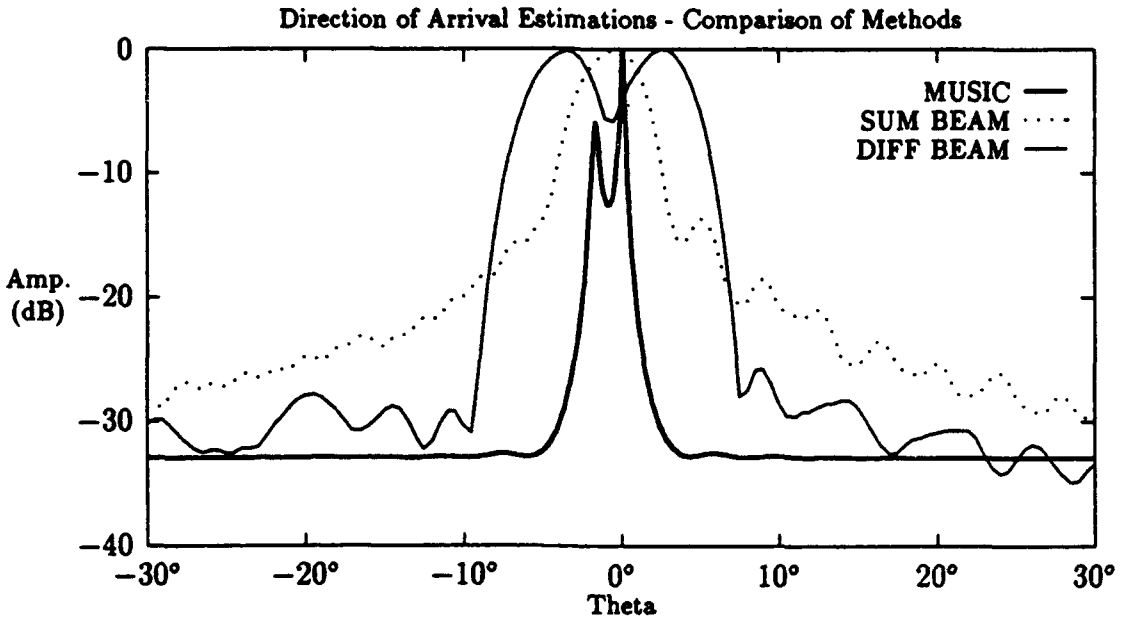

Figure 18: Comparison of DOA Estimations - Sources 1.7° apart

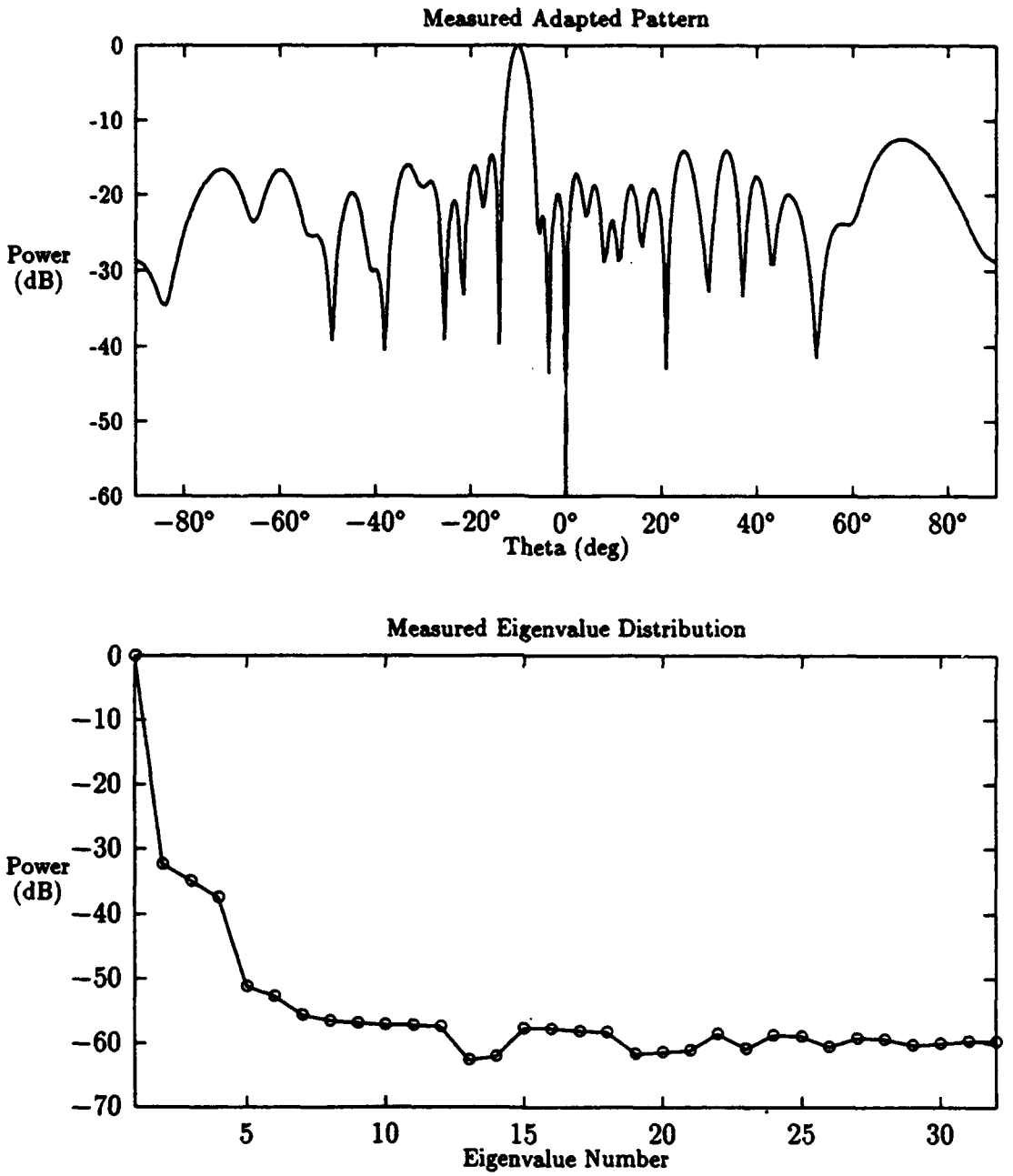

Figure 19: Adapted Pattern and Corresponding Covariance Matrix Eigenvalues

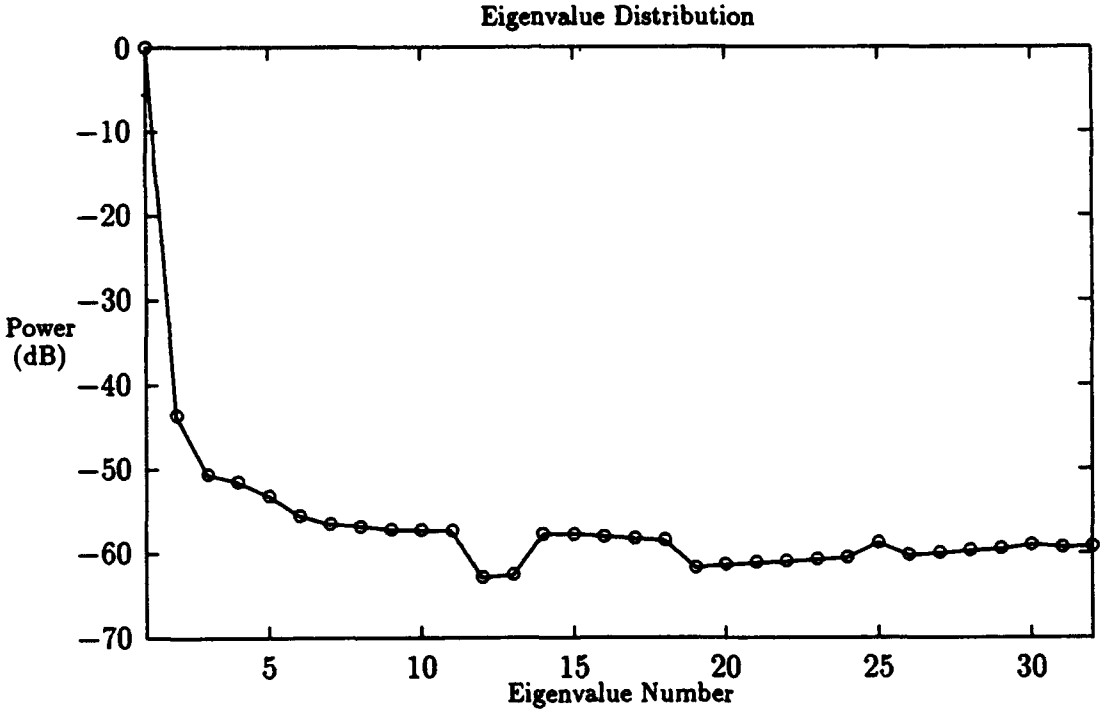

Figure 20: Covariance Matrix Eigenvalues after Correction of dc Offset, I/Q, and Third Harmonic Errors

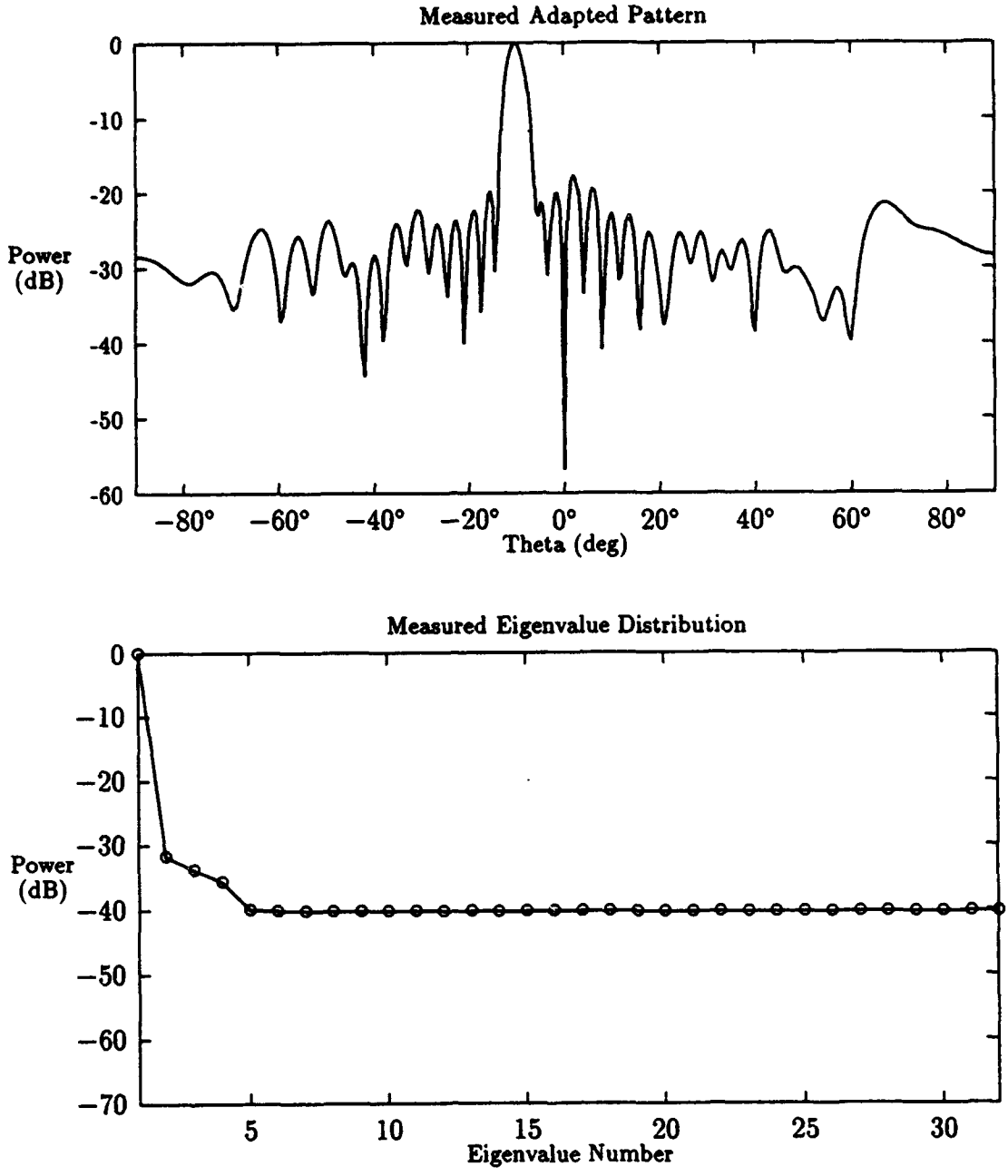

Figure 21: Adapted Pattern and Corresponding Covariance Matrix Eigenvalues - diagonally loaded

5 CONCLUSIONS

The purpose of this document was to provide a recent evaluation of the digital beamforming testbed at Rome Laboratory. In doing so, we have completely documented the dominant errors associated with the array's receive system. We have described the spectral and eigen analysis methods used to isolate and analyze the errors as well as illustrate their effects on the antenna pattern. In addition, we have successfully demonstrated the ability to implement the MUSIC and SMI algorithms used for super resolution and adaptive nulling capabilities. As a result, we have illustrated enhanced array performance and the flexibilty and power associated with digital beamforming.

References

[1] Applebaum, S.P. (1976) Adaptive arrays. *IEEE Transactions on Antennas and Propagation*, pages 585–598,

[2] Eber, Louis (1988) Digital Beam Steering Antenna. Technical Report RADC-TR-88-83, Rome Laboratory, AD A200 030

[3] Langston, J. Leland (1988) Design Definition for a Digital Beamforming Processor. Technical Report RADC-TR-88-86, Rome Laboratory, AD A196 983

[4] Pettersson, Lars Emil (1992) Adaptive Beamforming with Imperfect Arrays: Pattern Effects and Their Partial Correction. Technical Report RL-TR-92-341, Rome Laboratory, AD A267 079

[5] Schmidt, R. (1986) Multiple Emitter Location and Parameter Estimation. *IEEE Transactions on Antennas and Propagation*, pages 276–280,

MISSION

OF

ROME LABORATORY

Rome Laboratory plans and executes an interdisciplinary program in research, development, test, and technology transition in support of Air Force Command, Control, Communications and Intelligence (C3I) activities for all Air Force platforms. It also executes selected acquisition programs in several areas of expertise. Technical and engineering support within areas of competence is provided to ESC Program Offices (POs) and other ESC elements to perform effective acquisition of C3I systems. In addition, Rome Laboratory's technology supports other AFMC Product Divisions, the Air Force user community, and other DOD and non-DOD agencies. Rome Laboratory maintains technical competence and research programs in areas including, but not limited to, communications, command and control, battle management, intelligence information processing, computational sciences and software producibility, wide area surveillance/sensors, signal processing, solid state sciences, photonics, electromagnetic technology, superconductivity, and electronic reliability/maintainability and testability.